Mechanistic modeling of the effects of myoferlin on tumor cell invasion

Marisa C. Eisenberg[a,1], Yangjin Kim[b], Ruth Li[c], William E. Ackerman[c], Douglas A. Kniss[c,d], and Avner Friedman[a,e,1]

[a]Mathematical Biosciences Institute, Ohio State University, Columbus, OH 43210; [b]Department of Mathematics, University of Michigan, Dearborn, MI 48128; [c]Department of Obstetrics and Gynecology, Ohio State University, Columbus, OH 43210; [d]Department of Biomedical Engineering, Ohio State University, Columbus, OH 43210; and [e]Department of Mathematics, Ohio State University, Columbus, OH 43210

Contributed by Avner Friedman, October 5, 2011 (sent for review August 18, 2011)

Myoferlin (MYOF) is a member of the evolutionarily conserved ferlin family of proteins, noted for their role in a variety of membrane processes, including endocytosis, repair, and vesicular transport. Notably, ferlins are implicated in *Caenorhabditis elegans* sperm motility (Fer-1), mammalian skeletal muscle development and repair (MYOF and dysferlin), and presynaptic transmission in the auditory system (otoferlin). In this paper, we demonstrate that MYOF plays a previously unrecognized role in cancer cell invasion, using a combination of mathematical modeling and in vitro experiments. Using a real-time impedance-based invasion assay (xCELLigence), we have shown that lentiviral-based knockdown of MYOF significantly reduced invasion of MDA-MB-231 breast cancer cells in Matrigel bioassays. Based on these experimental data, we developed a partial differential equation model of MYOF effects on cancer cell invasion, which we used to generate mechanistic hypotheses. The mathematical model predictions revealed that matrix metalloproteinases (MMPs) may play a key role in modulating this invasive property, which was supported by experimental data using quantitative RT-PCR screens. These results suggest that MYOF may be a promising target for biomarkers or drug target for metastatic cancer diagnosis and therapy, perhaps mediated through MMPs.

cancer invasion | RNAi | partial differential equation models | metastasis

A majority of cancer deaths are related not to the primary tumor itself, but rather the formation of disseminated metastases (1). Cancer spread requires that cells achieve atypical motility, which enables them to invade surrounding tissues and vessels of the blood and lymphatic systems (2–4). Thus, understanding the mechanisms and signaling processes that lead to invasive cell behavior may lead to new therapeutic approaches for controlling and treating cancer.

The fundamental mechanisms of invasive cancer cell movement are largely conserved across a wide range of cell types, with some of the protease dependent and protease independent movement types demonstrated by cancer cells also seen in organisms as diverse as unicellular organisms, slime molds, and white blood cells. The ferlin family is an evolutionarily ancient family of proteins (5), which are known to affect processes crucial to migration and invasion, including membrane fusion and repair, vesicle transport, endocytosis, protein recycling and stability, and cell motility (6–13). Thus, one might expect the ferlin family to be good candidates for cancer proteins, although they have not previously been investigated in this capacity. In *Caenorhabditis elegans*, spermatozoa exhibit amoeboid movement, and mutations in the *fer-1* gene [an orthologue of myoferlin (MYOF)] result in immobility and infertility (13). In humans, MYOF has been implicated in a variety of cellular processes, including myoblast fusion, growth factor receptor stability, endocytosis, and endothelial cell membrane repair (6, 8, 10–12); however until now its role in cancer cell movement has not been explored. Although information on MYOF is currently limited, it has been shown to be upregulated in breast cancer biopsies (14) and expressed in breast cancer cell lines (15). Immunohistochemical evidence available from the Human Protein Atlas (16) suggests that MYOF is strongly expressed in several cancer types including colorectal, breast, ovarian, cervical, endometrial, thyroid, stomach, pancreatic, and liver cancer (14, 15, 17–26).

To explore the function of MYOF in cancer, a stable line of MYOF-deficient malignant breast carcinoma cells (MDA-MB-231) was generated using lentivirus-based delivery of shRNA constructs targeting human MYOF mRNA (Sigma). A stable, lentiviral control cell line was generated in tandem using lentiviral particles carrying a nonhuman gene targeting shRNA (Sigma). MYOF depletion was validated by immunoblotting (*SI Appendix*, Fig. 2). We used an electrode-impedance-based invasion assay [xCELLigence (27)] to probe the effect of MYOF deficiency on cell invasion. Compared to the control MBA-MB-231 cells, MYOF-knockdown (MYOF-KD) cells exhibited reduced invasive capacity (28).

Motivated by these experimental results, we developed a mathematical model that examines the role of MYOF in cancer cell invasion. Because relatively little is known about the function of MYOF in cancer, there is a useful opportunity for mathematical modeling to suggest hypotheses, which can then be tested experimentally. The model is described by a system of partial differential equations (PDEs). It builds on previous work on cancer cell migration/invasion (29), now incorporating a submodel for MYOF-mediated growth factor receptor recycling.

Using multiple MYOF-related datasets (8–12), we determined several parameters which differed between wild-type/control and MYOF-deficient cells. Our simulations suggest that one key parameter—the matrix metalloproteinase (MMP) production rate—is enough to reproduce the experimental data showing reduced MYOF-KD cell invasion. Based on the mathematical model, we hypothesized that MYOF affects MMP production and/or secretion in MDA-MB-231 cells. Preliminary experimental results thus far confirm our hypothesis. Indeed, pilot PCR results presented in this work show that MMPs may be significantly downregulated by MYOF depletion.

We propose that MYOF may serve as a fundamental player in cancer cell movement, by regulating the local behavior of the plasma membrane and affecting trafficking of receptors and proteins to and from the membrane. In particular, MYOF effects on MMP production and release may be key to its role in regulating tumor cell invasivity. Metastasis requires cancer cells to develop increased invasive capability, suggesting that MYOF may play an important role in the ability of tumor cells to metastasize.

Author contributions: M.C.E., Y.K., R.L., W.E.A., D.A.K., and A.F. designed research, performed research, and wrote the paper.

The authors declare no conflict of interest.

[1]To whom correspondence may be addressed. E-mail: meisenberg@mbi.osu.edu or afriedman@mbi.osu.edu.

This article contains supporting information online at www.pnas.org/lookup/suppl/doi:10.1073/pnas.1116327108/-/DCSupplemental.

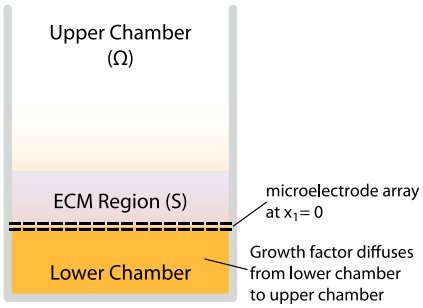

Fig. 1. xCELLigence well setup. The upper (Ω) and lower chambers are separated by a semipermeable membrane and microelectrode array at $x_1 = 0$. Matrigel/ECM sits on top of the microelectrode array (indicated by region S).

Mathematical Model

Spatial Setup. The conventional modified Boyden chamber setup includes two chambers with a semipermeable membrane between them. There is typically laminin-rich matrix (e.g., Matrigel) on top of the semipermeable membrane, which replicates the ECM, and invasion is measured by the number of cells which invade through the matrix and cross the membrane from the upper to the lower chamber. For the xCELLigence data, the membrane is coupled with a microelectrode array at the bottom of the upper chamber. Cells begin in the upper chamber (Ω in Fig. 1), from where they can migrate and invade through the ECM (region S in Fig. 1) to reach the microelectrode array. They then cross the membrane/microelectrode array and attach to the bottom side of the array upon crossing. Growth factors (GF) may be introduced in the bottom well below the microelectrode array, to act as a chemoattractant for the cells.

We measure the approximate number of cells which have adhered to the microelectrode array by measuring the change in impedance, the cell index [although we note that cell index is also dependent on other factors, such as cell adhesion and spreading (27)]. To simulate these conditions, we can use a similar setup as for the conventional modified Boyden chamber simulations given in refs. 29 and 30, with several modifications to incorporate the microelectrode array and measurement of cell index. Full mathematical description and details on the spatial setup and boundary/initial conditions are given in *SI Appendix*.

State Variable Definitions. We introduce the following variables:

R_1, free growth factor receptor (GFR) (number/cell)
R_2, surface-bound GF-GFR complex (number/cell)
R_3, internalized GF-GFR complex (number/cell)
ρ, concentration of ECM (g/cm^3)
P, MMP concentration (g/cm^3)
G, GF concentration (g/cm^3)
n, density of breast cancer cells (cells/cm^3)

Although MMPs are a diverse family of proteins with overlapping yet distinct functions, for simplicity we model their combined effects with the variable P, which represents generic/nonspecific MMP concentration. Similarly, because our experimental data use fetal calf serum as a chemoattractant, the variable G represents a combination of multiple growth factors (further details given in *SI Appendix*).

Model Equations. The model equations are based on the model variable interactions shown in Fig. 2. MYOF has been shown in other contexts to affect membrane processes (6, 8, 11) and receptor/protein recycling/transport (10, 12). Parameters relating to these functions, e.g., receptor recycling parameters, are underlined in Eqs. **1**–**7**, indicating they are considered MYOF-dependent. We developed two versions of the cell-related parameters—one for wild-type/control cells and another for MYOF-KD cells, as described below.

$$\frac{\partial R_1}{\partial t} = (\underline{\lambda}_1 - k_{21}R_1G + \underline{k}_{13}R_3 - \underline{k}_{01}R_1)\frac{n}{n_0} \quad [1]$$

$$\frac{\partial R_2}{\partial t} = (k_{21}R_1G - \underline{k}_{32}R_2 + \underline{k}_{23}R_3)\frac{n}{n_0} \quad [2]$$

$$\frac{\partial R_3}{\partial t} = [\underline{k}_{32}R_2 - (\underline{k}_{13} + \underline{k}_{23} + \underline{k}_{03})R_3]\frac{n}{n_0} \quad [3]$$

$$\frac{\partial \rho}{\partial t} = \underbrace{-\lambda_{21}P\rho}_{\text{degradation}} + \underbrace{\lambda_{22}\rho\left(1 - \frac{\rho}{\rho_0}\right)}_{\text{reconstruction(small)}} \quad \text{in } S \quad [4]$$

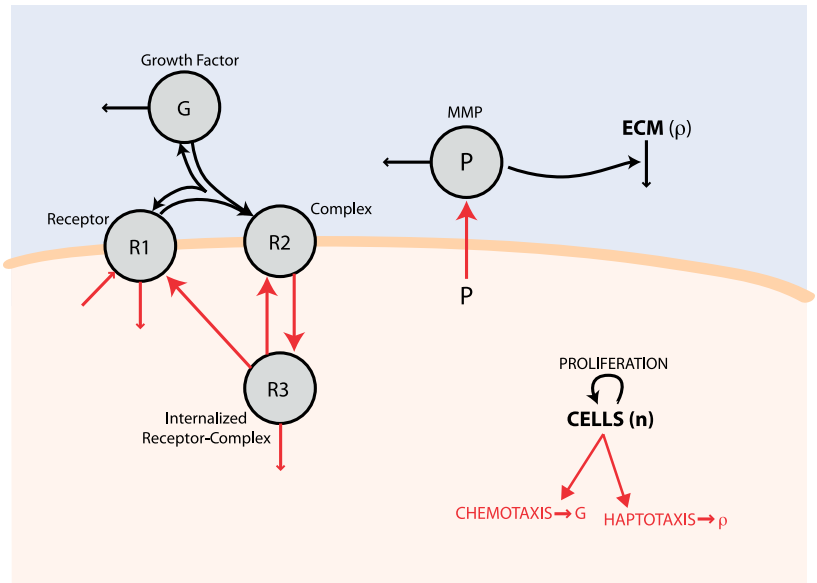

Fig. 2. Model for receptor recycling and cell migration and invasion, with processes marked in red affected by MYOF. Cells (n) proliferate, migrate, and invade following these processes, with cell movement dependent on the growth factor gradient (chemotaxis) and the extracellular matrix gradient (haptotaxis).

$$\frac{\partial P}{\partial t} = D_p \nabla^2 P + \underbrace{\underline{\lambda_{31}} n\rho}_{\text{production by cells}} - \underbrace{\underline{\lambda_{32}} P}_{\text{degradation}} \quad [5]$$

$$\frac{\partial G}{\partial t} = D_G \nabla^2 G - \underbrace{\underline{k_{21}} C_{mw} R_1 n G}_{\text{binding}} - \underbrace{\underline{\lambda_{10}} G}_{\text{degradation}} \quad [6]$$

$$\frac{\partial n}{\partial t} = D_n \nabla^2 n + \underbrace{\underline{\lambda_{11}} n(1 - \frac{n}{n_0} - \mu\rho)\frac{R_2}{R_{20}}}_{\text{proliferation}}$$

$$- \nabla \cdot \left(\underbrace{\underline{\chi_n} \frac{n \frac{R_2}{R_{20}} \nabla G}{\sqrt{1 + \lambda_G |\nabla G|^2}}}_{\text{chemotaxis}} + \underbrace{\underline{\chi'_n} I_S \frac{n \nabla \rho}{\sqrt{1 + \lambda_\rho |\nabla \rho|^2}}}_{\text{haptotaxis}} \right) \quad [7]$$

Eqs. **1–3** constitute the receptor recycling ordinary differential equation (ODE) submodel, collectively representing growth factor receptor binding, internalization, degradation, and return to the cell surface. We assume that all the internalized ligand is degraded so that ligand return to the surface may be neglected. The receptor recycling submodel equations are multiplied by n/n_0 to scale the concentrations to the local cell density.

The remaining PDEs are largely based on a previous model of tumor growth and movement in a Boyden chamber (29), updated and with modifications to incorporate MYOF effects and our particular experimental setup. The ECM, in Eq. **4**, undergoes degradation by MMP (31) and includes a small remodeling term (30, 32–34). In Eq. **5**, MMP is produced by the cells to degrade the matrix, and then degrades and diffuses. Because MMP is produced in response to the presence of extracellular matrix, we have modified this term from ref. 29 to be dependent on both n and ρ. Growth factor in Eq. **6** diffuses from below the xCELLigence well bottom, where it binds to free receptors on the cell surface, and is degraded at a constant rate.

Lastly, tumor cells Eq. **7** begin above the ECM in the upper chamber, from which they then undergo dispersion, chemotaxis following the GF concentration gradient, haptotaxis through the ECM, following the ECM concentration gradient, and growth factor dependent proliferation based on the level of surface-bound growth factor (Fig. 2). Cell proliferation is modeled as logistic growth, to which we add an additional ECM-dependent term to account for additional crowding effects in the presence of ECM (35). The diffusion constants and other parameters are positive constants.

Parameter Estimation. As discussed above, MYOF is known to affect a variety of membrane processes (6, 8, 11) and receptor/protein recycling and transport (10, 12). Thus, we developed two versions of the membrane-related model parameters, underlined in Eqs. **1–7**, each characterizing the wild-type/lentiviral control and MYOF-KD cell types represented in our study.

The two versions of the receptor recycling submodel parameters in Eqs. **1–3** were determined by fitting to experimental receptor internalization data from wild-type and MYOF-null myoblasts [MYOF knockout (MYOF-KO)] cells (12), with the full details of the model parameterization given in *SI Appendix*. The resulting parameter estimates suggest that MYOF-deficient cells yield decreased GFR production, and increased receptor recycling pathways leading to receptor degradation.

There are three MYOF-dependent parameters in the full PDE model which remain unaccounted for—the MMP secretion rate and the chemotactic and haptotactic sensitivity parameters. As MYOF-KD cells show decreased invasivity compared to wild-type/control cancer cells, we expect these parameters to decrease in the MYOF-KD case. The ODE submodel parameters show between a 13 and 40% change between wild-type and MYOF-KD parameter values, so we suppose $\chi_{nm} = 0.75\chi_n$ and $\chi'_{nm} = 0.75\chi'_n$. As MMP has been shown to associate with MYOF (36) and MMP secretion is directly membrane-related, we would expect that λ_{31} will be more strongly affected by the MYOF-KD. Indeed, we found the best fits to the xCELLigence invasion data for a significantly lower value of λ_{31m}, so that we take $\lambda_{31m} = \lambda_{31}/100$. The remaining non-MYOF-dependent PDE model parameters for both the wild-type/control and MYOF-KD cells were determined based on literature values (29, 30, 36, 37) (see *SI Appendix*, Tables 1 and 2 for individual references).

Simulation Results. The overall model behavior for the wild-type/control and MYOF-KD cells in the xCELLigence wells with 20% Matrigel coating are shown in *SI Appendix*, Figs. 3 and 4. Tumor cell invasion is more significant in wild-type/control than MYOF-KD cells, matching experimental data. Bound and internalized receptors tend to follow the invading front of tumor cells, with cells toward the top of the upper well tending to have more unbound receptors (as the GF has not diffused completely up the chamber). MMP also tends to roughly follow the invading front of tumor cells, as does degradation of ECM, with MMP production dropping off outside the ECM region.

Applications to Cancer Cell Invasion

Decreased Invasion in MYOF-KD Cells. Figs. 3 and 4 show model simulations compared to cell index experimental data in xCELLigence wells for wild-type/control and MYOF-KD cells at 20% and 100% Matrigel concentrations. Model simulations recover the qualitative behavior of the experimental data, with a more significant decrease in invasivity for MYOF-KD cells in 100% Matrigel compared to 20% Matrigel.

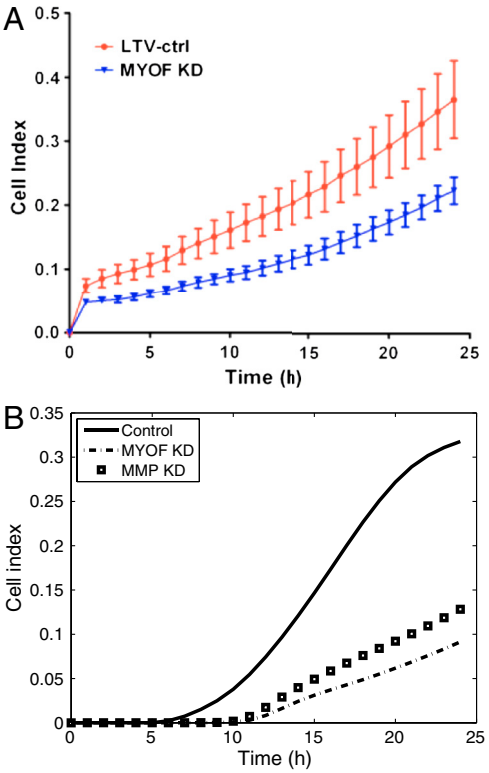

Fig. 3. Comparison between experimental data and simulation results with 20% Matrigel. (*A*) Experimental results for lentiviral control (LTV-ctrl) and MYOF-KD cells. (*B*) Simulation results for wild-type/control, MYOF-KD, and hypothetical MMP KD cells.

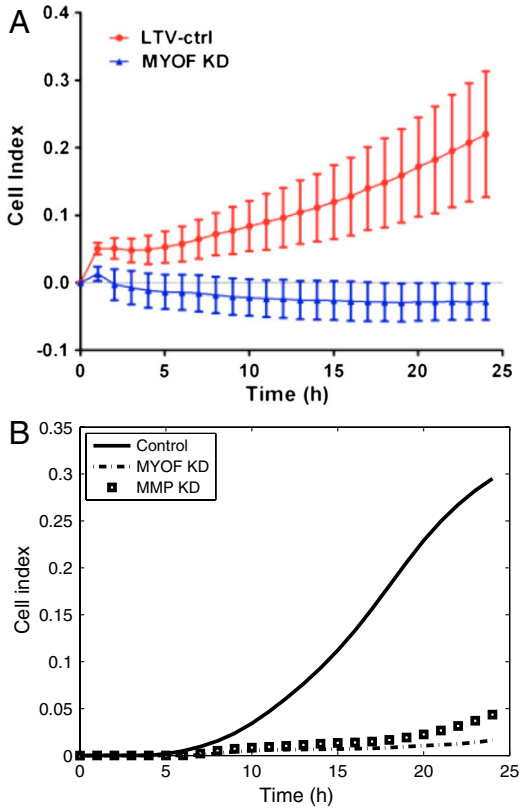

Fig. 4. Comparison between experimental data and simulation results with 100% Matrigel. (*A*) Experimental results for lentiviral control (LTV-ctrl) and MYOF-KD cells. (*B*) Simulation results for wild-type/control, MYOF-KD, and hypothetical MMP KD.

MMP is a Key Target for Myoferlin Effects. We also simulated the cell index for a hypothetical MMP-KD case, where the model parameters were fixed at wild-type/control values except for the MMP production rate, λ_{31}, which was set equal to the decreased MYOF-KD value λ_{31m}. We found that loss of MMP alone was enough to account for most of the changes in cell invasivity seen in MYOF-KD cells (Figs. 3 and 4).

Preliminary Experimental Validation. Based on these results, we used a PCR array to examine whether MYOF depletion affects MMPs. We found that MMP1 was over 100-fold downregulated in MYOF-KD MDA-MB-231 cells compared to lentiviral controls, matching the model predictions and suggesting that MMPs may indeed be a target of MYOF. Additionally, MYOF has been found to be a substrate for membrane type 1 MMP (MT1-MMP) in MDA-MB-231 cells (38). These results serve to partially validate our simulation predictions that MMP may be important to MYOF effects on cell invasion.

Myoferlin and Receptor Tyrosine Kinases (RTKs). Because MYOF has been shown to stabilize RTKs such as Tie-2, insulin-like growth factor (IGF) receptors and VEGF receptors (10, 12, 39), we hypothesized that MYOF may provide a generalized mechanism of RTK (and other receptor) stabilization in cancer cells, perhaps by modulating receptor recycling so that vesicles are targeted for recycling rather than the lysosomal degradation pathway [as suggested for myoblast fusion and muscle growth in (12)]. Thus, we modeled MYOF effects using a generalized receptor, where MYOF-KD affects the recycling/degradation rates for internalized receptors. Preliminary experimental results confirm that phosphorylated forms of several RTKs (EphB4, FGFR2, Hck, IGF-1R, JAK2, tyrosine protein kinase, and VEGFR2) are significantly downregulated in MYOF-KD MDA-MB-231 cells (*SI Appendix*, Fig. 5).

Predictive Simulations of Myoferlin Effects on Chemotaxis and Haptotaxis. Next, we simulated varying concentrations of Matrigel (P) and growth factor (G) to explore how wild-type/control and MYOF-KD cells may behave under a range of experimental conditions. We simulated varying ECM concentrations from 10–100%, and growth factor concentrations for 0.5, 1, and 2 times normal. Simulated MYOF-KD cells showed a more dramatic decrease in invasion than wild-type/control cells, consistent with the significant effects on invasion related parameters in the model (*SI Appendix*, Fig. 6). By contrast, the effects of varying GF were relatively small in both wild-type and MYOF-KD simulations. Simulated MYOF-KD cell invasion was less affected than wild-type/control simulations, perhaps as a result of the decreased sensitivity of MYOF-KD cells to GF due to changes in chemotactic sensitivity and growth factor receptor recycling (*SI Appendix*, Fig. 7).

In Vivo Tumor Growth Simulations. All the models and experimental data persented here thus far have considered cells in vitro. However, we can use the model to explore hypothetical cancer cell behavior in a simulated tumor in vivo, and in particular, to examine how a heterogeneous microenvironment affects cell invasion. We simulated a two-dimensional scenario of a clump of wild-type or MYOF-KD tumor cells surrounded by ECM, using differing diffusion coefficients (normal and 1/10 normal based on *SI Appendix*, Table 1) on the left and right halves of the domain. In wild-type cells, cell invasion was significantly reduced for lower diffusion coefficients (*SI Appendix*, Fig. 8). MMP followed the invading front of tumor cells, as in the xCELLigence wells simulations. Although GF concentrations were fairly similar for both halves of the domain, bound, unbound, and internalized GF receptor concentrations were quite different for the two diffusion coefficient values. For MYOF-KD cells, tumor invasion was markedly less than in the wild-type case, so that after 24 h, the tumor cells had not significantly invaded the surrounding tissue (*SI Appendix*, Fig. 9). MMP, ECM, and GF levels change less than in the wild type case, and the differences between the two diffusion coefficient microenvironments were less evident, likely due to decreased overall invasion.

Discussion

MYOF belongs to the evolutionarily ancient ferlin family, which has been associated with a variety of processes important to cell migration and invasion, such as cell motility, growth factor receptor stability, endocytosis, and membrane repair (7–10, 11, 13). Although MYOF and the ferlin family have not previously been studied for their role in cancer, several reports suggest an association between MYOF overexpression and metastatic cancer (14, 15, 17–26). In this work we used a combination of mathematical modeling and experimental validation to uncover MYOF as a cancer protein, which we propose may be involved in regulating cancer cell invasion.

We developed a PDE model of MYOF-mediated cancer cell invasion, as a tool to generate hypotheses regarding the mechanisms behind MYOF effects on breast cancer cell invasion. The model extends existing models of cancer cell movement (29, 30) to incorporate receptor recycling and membrane regulatory effects of MYOF, based on experimental results using xCELLigence assays (27) showing that MYOF-KD MDA-MB-231 cells exhibited decreased invasivity (Figs. 3 and 4, with immunoblot validation of MYOF specific depletion shown in *SI Appendix*, Fig. 2).

Model simulations confirm the experimental observation of decreased invasion in MYOF-KD cells (Figs. 3 and 4), and predictive simulations suggest that MYOF-KD cells may be less

able to invade (and thus metastasize) in vivo as well. The model simulations also suggest that the effects of MYOF on cell invasion may be in large part mediated by MMPs, as similar invasion profiles could be obtained in simulation by MYOF-mediated loss of MMP production/secretion alone. Based on these predictions, we proposed that MMPs may be key targets of MYOF, and that the effects of MYOF-KD on tumor cell invasiveness may be due in large part to the loss of MYOF effects on MMP production and/or secretion.

These modeling results led us to survey MMP expression following MYOF-KD. We used quantitative RT-PCR arrays to examine gene regulatory changes in MYOF-KD cells, and found an unexpected link between MYOF and MMPs, namely that loss of MYOF results in 100-fold downregulation of MMP-1, matching model predictions. These results confirm that MYOF does indeed have a significant effect on MMP, and highlight how interactions between experiments and mathematical modeling can provide a fruitful method for generating and testing hypotheses.

In this model we also hypothesized that MYOF may provide a generalized mechanism of RTK stabilization in cancer cells, perhaps via changes in the receptor recycling/degradation pathways (motivated by ref. 12). We have partially confirmed this hypothesis using RTK phosphorylation arrays (*SI Appendix*, Fig. 5). Although the present paper is focused on cancer cell invasion, this process is only one facet of the larger picture of metastasis, which involves a wide variety other processes (including migration, angiogenesis, and proliferation at secondary sites). Subsequent work in progress on migration and other aspects of MYOF in cancer provide an opportunity for this generalized model to be specialized for individual receptors and the interactions between MYOF and RTKs to be further examined.

To conclude, MYOF appears to be a promising target in cancer therapy. Our mathematical and experimental results highlight the connection between membrane trafficking processes and cell invasion, and suggest that MYOF plays a significant role in promoting invasive behavior. Moreover, based on our model predictions together with preliminary experimental validation, we propose that MYOF may play a significant role in regulating MMPs in cancer. Indeed, based on our model predictions, we hypothesize that these effects on MMPs are an important component of the regulatory changes associated with MYOF. Previous studies (29, 40, 41) have highlighted the effects of the tumor microenvironment on cell movement, suggesting that modulating cell adhesion or blocking MMPs may be a way to control and treat cancer. MYOF may be a promising target for such therapeutic approaches, or perhaps a biomarker for metastasis. As more information about the regulatory network of MYOF in cancer is uncovered, our model may be extended to include a dynamic equation for MYOF within a larger protein network, and used to further test potential therapeutic targets.

Materials and Methods

Mathematical Modeling Methods. All model simulations were performed using a finite volume method and clawpack (http://www.amath.washington.edu/~claw/) with fractional step method (42) as well as the nonlinear solver **nksol** for algebraic systems. The model equations were solved on a regular uniform spatial grid and an adaptive time step. Simulated cell index was assumed to be proportional to the fraction of cells that reach the well bottom, where we found a proportionality constant of 0.5 matched the experimental data well.

Cell Culture and Generation of Stably Transduced Cell Lines. MDA-MB-231 (American Type Culture Collection, HTB-26) cells were maintained in DMEM with 4.5 g/L D-glucose supplemented with 10% FBS. Recombinant lentiviral particles containing nontarget control shRNA (SHC002V) and human myoferlin (TRCN0000010628) targeted shRNA in the pLKO.1 vector were purchased from Sigma-Aldrich (MISSION). For lentiviral infection, cells were seeded in 24-well culture plates and incubated overnight at 37 °C in 5% CO_2 in a humidified atmosphere. Media was replaced with media containing 8 μg/mL hexadimethrine bromide (Sigma) and lentiviral particles were added to cultures that were approximately 70% confluent at a multiplicity of infection of 1. After overnight incubation (37 °C, 5% CO_2), virus-containing supernatant was removed and replaced with complete media and incubated overnight once more. Stably transduced cultures were selected in media containing an appropriate amount of puromycin as predetermined by a puromycin kill curve. Wild-type and MYOF-deficient cells were validated through short tandem repeat profiling at Johns Hopkins University's Fragment Analysis Facility.

Real-Time Invasion Monitoring. The invasion assays were completed on CIM-16 plates with 8 μm pore membranes (Roche). Wells were coated with 20 μL of 20% or 100% Matrigel and allowed to gel at 37 °C, 5% CO_2 for 4 h. After 4 h, the wells of the bottom chamber were filled with 160 mL of 10% serum containing media and the top and bottom portions of the CIM-16 plates were assembled together. The assembled CIM-16 plate was allowed to equilibrate for 2 h at 37 °C, 5% CO_2 after the addition of 50 μL of serum-free media to the top chamber wells. For seeding, cells were rinsed with PBS, trypsinized for 2 min, centrifuged at 150 g for 3 min, and washed with serum-free DMEM before resuspension in serum-free DMEM. Cells (8×10^4 cells/well) were seeded onto the top chambers of CIM-16 plates and placed into the xCELLigence system for data collection after a 30 min incubation at room temperature. The xCELLigence software was set to collect impendence data (reported as cell index) at least once every hour. Percentage invasion was calculated by the ratio of the cell index of invaded cells (with Matrigel coating) to the cell index of migrated cells (no Matrigel coating).

Quantitative RT-PCR Array. RT^2 Profiler PCR array from SABiosciences was performed for human extracellular matrix and adhesion molecules following manufacturer's protocol. Briefly, total RNA was extracted from lentiviral control and MYOF-deficient MDA-MB-231 cells that had been in culture for 10 consecutive passages using TRIzol reagent (Invitrogen), according to manufacturers' protocol up to the chloroform extraction and centrifugation steps. The resulting aqueous phase was mixed with an equal volume of 70% ethanol and applied to an RNeasy mini column (QIAGEN) and processed according to the manufacturer's protocol with DNase on column digestion. Total RNA was quantified with a NanoDrop 2000, and 1 μg of total RNA from each cell type was reverse-transcribed to cDNA using the RT^2 First Strand Kit (SABiosciences). Equal amounts of diluted cDNA was mixed with LightCycler 480 SYBR Green I Master mix (Roche) and aliquoted to each well of the PCR array plate containing the prefilled gene-specific primer sets, and PCR was performed according to manufacturer's instructions for the Roche LightCycler 480. The LightCycler 480 software (Roche) was used to calculate the threshold cycle (crossing point, Cp) values for all the transcripts in the array. The Cp values were then exported into an Excel-based PCR array data analysis template (SABiosciences) to calculate fold changes in gene expression for pairwise comparisons using the ΔΔCt method (where Ct is threshold cycle).

RTK Array. Initial screen of relative levels of phosphorylation of a panel of RTKs in MDA-MB-231 lentiviral control and MYOF-depleted cells were determined by an antibody array (RayBio Human RTK Phosphorylation Antibody Array 1, RayBiotech, Inc.), using 600 μg/mL of protein for each cell type and following the manufacturer's protocol. The membranes were quantified by densitometry (Quantity One software, BioRad), with global background substraction of the average value of negative control spots on the array.

ACKNOWLEDGMENTS. This work was supported in part by National Science Foundation Award 0635561 (to M.E.), Ohio State University Perinatal Research and Development Fund (D.A.K., W.E.A., R.L.), K08 HD49628 (to W.E.A.), National Science Foundation Award EEC-0425626 (to R.L.), and Roche Applied Science (D.A.K., W.E.A.).

1. Eccles SA, Welch DR (2007) Metastasis: Recent discoveries and novel treatment strategies. *Lancet* 369:1742–1757.
2. Howlett NG, et al. (2002) Biallelic inactivation of BRCA2 in fanconi anemia. *Science* 297:606–609.
3. Thiery JP, Acloque H, Huang RY, Nieto MA (2009) Epithelial-mesenchymal transitions in development and disease. *Cell* 139:871–890.
4. Lopez-Novo JM, Nieto A (2009) Inflammation and EMT: An alliance towards organ fibrosis and cancer progression. *EMBO Mol Med* 1:303–314.
5. Lek A, Lek M, North K, Cooper S (2010) Phylogenetic analysis of ferlin genes reveals ancient eukaryotic origins. *BMC Evol Biol* 10:231.
6. Doherty KR, et al. (2008) The endocytic recycling protein EHD2 interacts with myoferlin to regulate myoblast fusion. *J Biol Chem* 283:20252–20260.

7. Davis DB, Doherty KR, Delmonte AJ, McNally EM (2002) Calcium-sensitive phospholipid binding properties of normal and mutant ferlin C2 domains. *J Biol Chem* 277:22883–22888.
8. Cipta S, Patel HH (2009) Molecular bandages: Inside-out, outside-in repair of cellular membranes. Focus on "myoferlin is critical for endocytosis in endothelial cells". *Am J Physiol Cell Physiol* 297:C481–C483.
9. Davis DB, Delmonte AJ, Ly CT, McNally EM (2000) Myoferlin, a candidate gene and potential modifier of muscular dystrophy. *Hum Mol Genet* 9:217–226.
10. Bernatchez PN, et al. (2007) Myoferlin regulates vascular endothelial growth factor receptor-2 stability and function. *J Biol Chem* 282:30745–30753.
11. Bernatchez PN, Sharma A, Kodaman P, Sessa WC (2009) Myoferlin is critical for endocytosis in endothelial cells. *Am J Physiol Cell Physiol* 297:C484–C492.
12. Demonbreun AR, et al. (2010) Myoferlin is required for insulin-like growth factor response and muscle growth. *FASEB J* 24:1284–1295.
13. Nelson GA, Roberts TM, Ward S (1982) *Caenorhabditis elegans* spermatozoan locomotion: Amoeboid movement with almost no actin. *J Cell Biol* 92:121–131.
14. Amatschek S, et al. (2004) Tissue-wide expression profiling using cDNA subtraction and microarrays to identify tumor-specific genes. *Cancer Res* 64:844–856.
15. Adam PJ, et al. (2003) Comprehensive proteomic analysis of breast cancer cell membranes reveals unique proteins with potential roles in clinical cancer. *J Biol Chem* 278:6482–6489.
16. Ponten F, Jirstrom K, Uhlen M (2008) The human protein atlas—a tool for pathology. *J Pathol* 216:387–393.
17. van't Veer LJ, et al. (2002) Gene expression profiling predicts clinical outcome of breast cancer. *Nature* 415:530–536.
18. Stec J, et al. (2005) Comparison of the predictive accuracy of DNA array-based multigene classifiers across cDNA arrays and Affymetrix GeneChips. *J Mol Diagn* 7:357–367.
19. DeNardo DG, et al. (2005) Global gene expression analysis of estrogen receptor transcription factor cross talk in breast cancer: Identification of estrogen-induced/activator protein-1-dependent genes. *Mol Endocrinol* 19:362–378.
20. Labhart P, et al. (2005) Identification of target genes in breast cancer cells directly regulated by the SRC-3/AIB1 coactivator. *Proc Natl Acad Sci USA* 102:1339–1344.
21. Iacobuzio-Donahue CA, et al. (2003) Exploration of global gene expression patterns in pancreatic adenocarcinoma using cDNA microarrays. *Am J Pathol* 162:1151–1162.
22. Zhao C, Putnik M, Gustafsson JA, Dahlman-Wright K (2009) Microarray analysis of altered gene expression in ERbeta-overexpressing HEK293 cells. *Endocrine* 36:224–232.
23. Kristiansen G, et al. (2005) Expression profiling of microdissected matched prostate cancer samples reveals CD166/MEMD and CD24 as new prognostic markers for patient survival. *J Pathol* 205:359–376.
24. Skubitz AP, Pambuccian S, Argenta P, Skubitz K (2006) Differential gene expression identifies subgroups of ovarian carcinoma. *Transl Res* 148:223–248.
25. Hasegawa S, et al. (2002) Genome-wide analysis of gene expression in intestinal-type gastric cancers using a complementary DNA microarray representing 23,040 genes. *Cancer Res* 62:7012–7017.
26. Ma C, et al. (2008) Mycobacterium tuberculosis culture supernatant induces cancer cell apoptosis and cell cycle arrest. *Open Cancer J* 2:31–41.
27. Bird C, Kirstein S (2009) Real-time, label-free monitoring of cellular invasion and migration with the xCELLigence system. *Nat Methods* 6:v–vi Application Note.
28. Li R (2011) The expression and effect of myoferlin depletion in breast cancer cells. PhD thesis (Ohio State University, Columbus, OH).
29. Kim Y, Friedman A (2009) Interaction of tumor with its micro-environment: A mathematical model. *Bull Math Biol* 72:1029–1068.
30. Kim Y, Friedman A, Wallace J, Li F, Ostrowski M (2009) Transformed epithelial cells and fibroblasts/myofibroblasts interaction in breast tumor: A mathematical model and experiments. *J Math Biol* 61:401–421.
31. Hansen R, Bissell M (2000) Tissue architecture and breast cancer: The role of extracellular matrix and steroid hormones. *Endocr Relat Cancer* 7:95–113.
32. Mueller M, Fusenig N (2004) Friends or foes—bipolar effects of the tumour stroma in cancer. *Nat Rev Cancer* 4:839–849.
33. Zhao Y, et al. (2004) Endometase/matrilysin-2 in human breast ductal carcinoma in situ and its inhibition by tissue inhibitors of metalloproteinases-2 and -4: A putative role in the initiation of breast cancer. *Cancer Res* 64:590–598.
34. Shiomi T, Okada Y (2003) MT1-MMP and MMP-7 in invasion and metastasis of human cancers. *Cancer Metastasis Rev* 22:145–152.
35. Perumpanani A, Byrne H (1999) Extracellular matrix concentration exerts selection pressure on invasive cells. *Eur J Cancer* 35:1274–1280.
36. Niiya D, et al. (2009) Identification and characterization of lutheran blood group glycoprotein as a new substrate of membrane-type 1 matrix metalloproteinase 1 (MT1-MMP). *J Biol Chem* 284:27360–27369.
37. Kim Y, Lawler S, Nowicki M, Chiocca E, Friedman A (2009) A mathematical model for pattern formation of glioma cells outside the tumor spheroid core. *J Theor Biol* 260:359–371.
38. Butler GS, Dean RA, Tam EM, Overall CM (2008) Pharmacoproteomics of a metalloproteinase hydroxamate inhibitor in breast cancer cells: Dynamics of membrane type 1 matrix metalloproteinase-mediated membrane protein shedding. *Mol Cell Biol* 28:4896–4914.
39. Yu C, et al. (2011) Myoferlin gene silencing decreases tie-2 expression in vitro and angiogenesis in vivo. *Vasc Pharmacol* 55:26–33.
40. Cheng J, Weiner L (2003) Tumors and their microenvironments: Tilling the soil. *Clin Cancer Res* 9:1590–1595.
41. Jones P (2001) Extracellular matrix and tenascin-c in pathogenesis of breast cancer. *Lancet* 357:1992–1994.
42. Tyson R, Stern L, LeVeque R (2000) Fractional step methods applied to a chemotaxis model. *J Math Biol* 41:455–475.